Nonspherical mirrors to reduce thermoelastic noise in advanced gravitational wave interferometers

Erika D'Ambrosio
California Institute of Technology, Pasadena, California 91125
(Received 11 December 2002; published 14 May 2003)

We introduce and study a non-Gaussian paraxial cavity mode that has a special beam intensity by properly designing the end mirrors of a resonator. The final aim is to reduce the thermoelastic noise generated by the interaction between the field and the mirror by optimizing the shape of both. We present numerical results for the special design of a resonator as long as the Fabry-Pérot arms of the gravitational wave detector Laser Interferometric Gravitational Wave Observatory (LIGO). We discuss the alignment stability of such a cavity and we present the most important investigations we have done for implementing the reshaped mirrors we propose in the next LIGO configuration. We implement different numerical tools in order to understand the impact of both a small misalignment in the Fabry-Pérot cavity and imperfections in the radial profile of the mirrors on the power built up inside the resonators and on the signal at the dark port of the beam splitter. The results of all the simulation runs are compared with an analytical model that takes into account mismatch problems and losses.

DOI: 10.1103/PhysRevD.67.102004 PACS number(s): 04.80.Cc, 07.05.Dz, 07.60.Ly, 42.55.−f

INTRODUCTION

In gravitational wave interferometric antennas, the variation of the distance between two mirrors is measured using the interference between the beams that come out of two perpendicular identical Fabry-Pérot cavities; one of them will sense a squeezing effect while the other will be stretched. The variation that is measured depends on any displacement of the reflective surfaces of the two mirrors. Such physical displacement can be caused by fundamental noise sources and it can also be mimicked by the measurement, because of any technical noise affecting the detection process.

In the design for the planned advanced Laser Interferometric Gravitational Wave Observatory (LIGO) interferometer, the mirror substrates are 40 kg sapphire cylinders. The most serious noise is thermoelastic noise (if fused silica substrates are used the considerations of this manuscript are irrelevant). The relevance of that kind of internal thermal noise has already been studied through mathematical models, for the infinite half-space approximation and for mirrors with finite size [1–3].

The intensity distribution of the electric field generates a heat flow, inside the mirror. The temperature inside the substrate is not homogeneous but varies on a small scale.

O'Shaughnessy and Thorne have pointed out that thermoelastic noise is reduced when the dynamically fluctuating bumps and valleys are averaged out by a flat laser beam instead of the baseline beam with Gaussian profile. It must also be a stable mode of the cavity, with a resonating frequency well separated by those of the higher order modes. A beam such as that is studied for a resonator as long as the arms of the LIGO gravitational wave antenna. This detector is briefly reviewed in Sec. I for comparison purposes with spherical mirrors. The flat topped beam is introduced in detail in Sec. II and the mirrors that support it as a resonating mode of the cavity are introduced.

Since those mirrors are considerably flatter than the baseline spherical mirrors, the sensitivity of the interferometer to errors in their orientation and shape is enhanced. The implications have been addressed by both analytical calculations and numerical simulations based on a fast Fourier transform (FFT) paraxial ray propagation code, using the flat topped mirrors [4,5].

In Sec. III we address a variety of problems related to misalignment. We consider realistic imperfections in the surface of the mirrors that affect the flat topped beam in Sec. IV. We tackle the main problems related to the quasidegeneracy of the recycling cavity and comment on some solutions.

I. OUTLINE OF GRAVITATIONAL WAVE INTERFEROMETERS WITH SPHERICAL MIRRORS

The reflected and transmitted electromagnetic field, for a cavity such as the one in Fig. 1, are defined by the transmittivities and reflectivities of the two end mirrors:

$$\psi_{ref}=\left(-r_1+\frac{t_1^2 r_2 e^{2ikL}}{1-r_1 r_2 e^{2ikL}}\right)\psi_{in}=r_{eff}\psi_{in},$$

$$\psi_{tr}=\frac{t_1 t_2 e^{ikL}}{1-r_1 r_2 e^{2ikL}}\psi_{in}=t_{eff}\psi_{in},$$

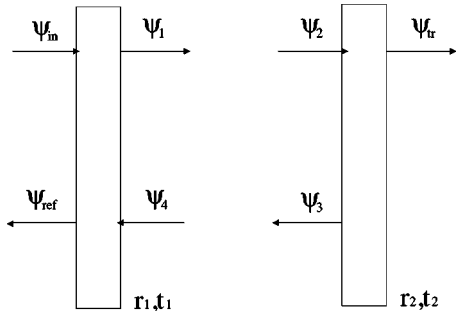

FIG. 1. Schematic diagram of a Fabry-Pérot cavity with front and back mirrors. In LIGO interferometers the mirrors are the gravitational masses under study: they have been conventionally named the internal and external test mass or ITM and ETM.

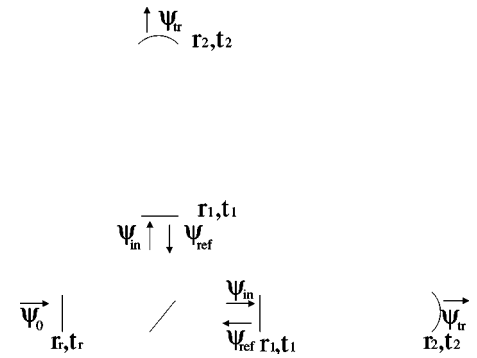

FIG. 2. The arm cavities and the recycling cavity.

where k is the wave number and L is the length of the resonator. We can add a recycling mirror so that the coupling between the two cavities is expressed by the effective reflectivity r_{eff}. Therefore we can write the power gain for the recycling cavity as

$$\mathrm{Gain}_{RC} = t_r^2/|1 - r_r r_{eff} e^{2ikl}|^2,$$

where l is the distance between the recycling mirror and the Fabry-Pérot cavity. We then introduce two Fabry-Pérot arms and a beam splitter as in Fig. 2.

If the beam splitter is perfect and the arms identical, the above formulas stand for the power circulating in the recycling cavity over the power that enters the interferometer through the recycling mirror. This ratio is the gain of the recycling cavity and it depends on the lengths l and L. The conditions for resonance are expressed by

$$e^{2ikL} = e^{2ikl} = 1.$$

Any difference in the effective reflectivities from the two arm cavities will be detected at the antisymmetric port of the beam splitter, which is also named the dark port or output port of the interferometer. The signal is proportional to δr_{eff}. If the only variation is caused by the gravitational wave,

$$\delta r_{eff} \simeq \frac{4i\mathcal{F}\phi_{gw}}{\pi}, \qquad \mathcal{F} = \frac{\pi\sqrt{r_1 r_2}}{1 - r_1 r_2},$$

with ϕ_{gw} the amplitude of the phase change predicted by the theory of general relativity, and $\mathcal{F}$ the finesse of the two Fabry-Pérot cavities.

The configuration we will focus on is the advanced LIGO (whose characteristics can be surveyed at www.ligo.caltech.edu/ligo2 [8]) and we are referring to its design for cavity lengths and mirror diameters. Reducing thermoelastic noise can be accomplished by increasing the spot size w of the Gaussian beams. This would result in increased diffraction losses, as a smaller portion of the field hits the surface of the mirror. The fraction of power that is lost may be expressed by the following formula:

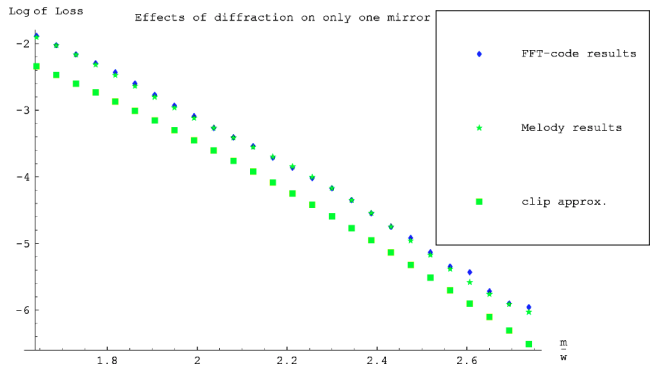

FIG. 3. Three sets of results for diffraction losses: two of them were obtained by a numerical code and one was computed by the amount of light that falls outside the mirror.

$$\mathcal{L} = \int_m^\infty \frac{2}{\pi w} \exp\left[-2\frac{r^2}{w^2}\right] 2r\pi dr = \exp\left[-2\frac{m^2}{w^2}\right],$$

m = half of the mirror's diameter,

based on the approximation that the field retains its shape. The finiteness of the mirrors may induce significant changes in the characteristics of the beam.

Using more sophisticated tools we can obtain different results for $\mathcal{L}$ [7].

The simple formula above is referred to as the clipping approximation. We computed $\mathcal{L}$ also using two different numerical codes (one based on the FFT of the field and one on its decomposition into transverse modes) and we found for both a result ~ 2.5 times larger than predicted by the clipping approximation as shown in Fig. 3. From the data we find that, setting the mirror's diameter at 30 cm, we have a diffraction loss of 10 ppm according to the design for the advanced LIGO, that is, using mirrors with radii of curvature 54 km in 4 km long Fabry-Pérot resonators. These parameters imply $w \sim 6$ cm for the size of the beam reflecting on the mirrors and are considered typical of the advanced LIGO configuration, as reported in www.ligo.caltech.edu/ligo2 [8].

A significant reduction of thermoelastic noise can be achieved by an increase of the spot size. Since this will cause larger diffraction losses, we can alternatively design a resonator with nonspherical mirrors, such that the fundamental mode sustained in there has a flat intensity profile with acceptable diffraction losses. This is proposed in the next section with a limit of 21 ppm on diffraction losses.

II. THE FLAT TOPPED BEAM AND THE CAVITY SUPPORTING IT AS AN OPTICAL MODE

We can overstep the limits put on Gaussian beams by the diffraction losses by using a non-Gaussian mode as proposed by O'Shaughnessy and Thorne, and studied by D'Ambrosio *et al.* [6]. We review the construction of that mode for a symmetric Fabry-Pérot cavity, which implies that the waist position is in the middle. We first define the intensity of the flat topped beam at its waist position, which is where the wave front is exactly flat, and we shall use a superposition of

Gaussian functions. The flattest intensity we may imagine is

$$u_s(x,y)=\begin{cases}\dfrac{1}{\sqrt{\pi p^2}} & \text{for} \quad x^2+y^2\leqslant p^2,\\ 0 \quad \text{for} & x^2+y^2>p^2,\end{cases}$$

which is a step function. We can obtain this by overlapping delta functions, and more generally a flat profile can be generated by overlapping narrow Gaussian functions as follows:

$$u_0(x,y)=\int\int_{x_0^2+y_0^2\leqslant p^2} dx_0 dy_0 \sqrt{\frac{2}{w_0^2\pi}} \times e^{-(1/w_0^2)\,[(x-x_0)^2+(y-y_0)^2]}$$

$$\text{when} \quad \frac{w_0}{p}\to 0, \tag{1}$$

but this is not the optimal choice. In fact, for each of the Gaussian beams overlapping to form the flat topped beam, the spot size becomes quite large in the propagation, making the field spread too much. So we have to choose a larger value for w_0 and keep the ratio w_0/p small. The minimum spot size on the mirrors of a Fabry-Pérot cavity is obtained for Gaussian beams whose waist is

$$w_0=\sqrt{\frac{L}{k}}=\sqrt{\frac{\lambda L}{2\pi}},$$

and this is the value we will use in Eq. (1). We make the beam propagate toward the end of the cavity, where one of the mirrors is located and we obtain

$$u(x,y)=\int\int_{x_0^2+y_0^2\leqslant p^2} dx_0 dy_0 \frac{1+i}{\sqrt{2w_0^2\pi}} \times e^{-[(1+i)/2w_0^2][(x-x_0)^2+(y-y_0)^2]} \tag{2}$$

as a result of

$$u(x,y)=\int dx' \int dy' K(x,y;x',y')u_0(x',y')$$

with the symmetric kernel

$$K(x,y;x',y')=\frac{2i}{\lambda L}\exp\left\{-\frac{2i\pi}{\lambda L}[(x-x')^2+(y-y')^2]\right\}.$$

Although $u(x,y)$ does not retain its shape, a definition of the Gouy phase is still possible as the phase gained by propagation along the longitudinal axis.

The field also has a wave front (the phase is not uniform on a plane transverse to the longitudinal axis).

We shall therefore define

$$\Phi_{WF}=\Phi[u(x,y)]-\Phi[u(0,0)]$$

and we can evaluate the wave front corresponding to the mirrors' location. When the flat topped beam hits a reflective surface that matches its wave front, the sign in front of Φ_{WF} is flipped so that when it is propagated back it has the same shape [9–11].

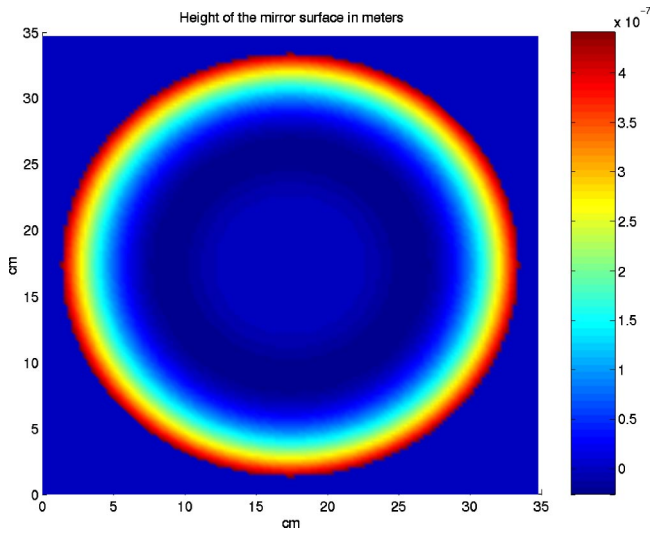

FIG. 4. The shape of mirrors supporting the flat topped beam is shown. The central area is significantly flat but on the external rim the surface is quite steep, reaching a height of about 0.5 μm in only $\sim$2 cm. The stability of the optical cavity formed by two of these mirrors 4 km apart is the main focus of the analytical and numerical studies reported in this paper.

In order to match the wave front of the beam, the height of the mirrors must be

$$h(x,y)=\frac{\lambda}{2\pi}\{\Phi[u(0,0)]-\Phi[u(x,y)]\}.$$

The corresponding profile for the end mirrors is shown in Fig. 4. The other way around, the fundamental mode of the cavity constructed according to this design must be a flat topped beam. In Fig. 5 the wave front of the beam resonating in such a cavity is shown. The phase map results from the FFT model we have been using. This numerical program simulates the propagation of the beam using the paraxial approximation. The first case we analyze is the ideal configuration with perfectly shaped and aligned mirrors. The appropriate information must be provided as input parameters; one preliminary calculation that we consider interesting is the design of the beam that drives the cavity.

A. Optimization of the beam profile for the field driving the cavity

We propose a technique to identify the Gaussian beam with the largest overlap with the field u. This analytical study is useful either to drive the system directly by a Gaussian beam or to maximize the laser power coupled inside the mode cleaner that prepares the field according to the flat topped profile. Any electromagnetic field is fully defined, once its transverse shape is known for one specific location. Therefore we evaluate the overlap at the waist position

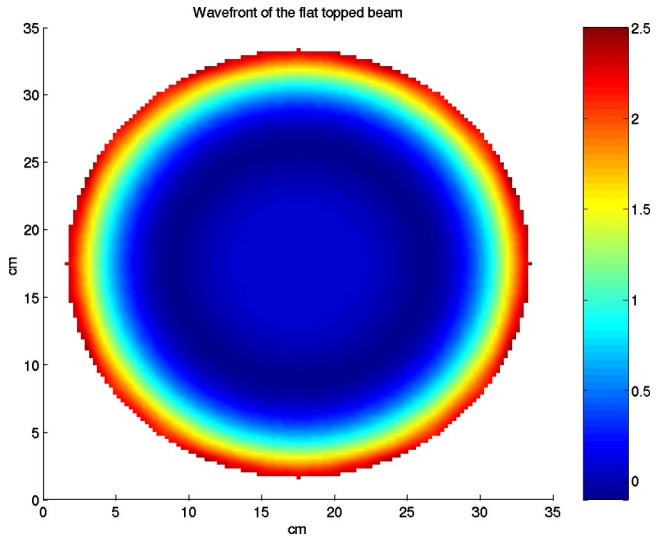

FIG. 5. The wave front of the flat topped beam, as computed by the maps of the real and imaginary parts of the electromagnetic field that resonates in the Fabry-Pérot cavity, simulated by the paraxial ray propagation code we have used to quantify the effect of a variety of perturbations on the stability of the system. Before analyzing practical issues we checked that the wave front of the flat topped beam resulting from the simulation corresponds to the profile we have designed. The numerical program makes the electromagnetic field bounce back and forth between the two mirrors until it converges toward the solution we expect: the flat topped beam whose wave front matches the profile of the end mirrors of the cavity

$$\mathcal{C}=\frac{\int\int dxdyu_G^*(x,y)u_0(x,y)}{\sqrt{\int\int dxdyu_0^2(x,y)}},$$

$$u_G(x,y)=\sqrt{\frac{2}{\pi w_G^2}}\exp\left[-\left(\frac{1}{w_G^2}+\frac{ik}{2R_G}\right)[x^2+y^2]\right],$$

and use the property

$$\begin{aligned}&\int\int dxdyu_G^*(x,y)u_0(x,y)\\&=\int\int dxdy\int\int dx'dy'u_G^*(x,y)\\&\quad\times\delta(x-x')\delta(y-y')u_0(x',y')\\&=\int\int dx''dy''\int\int dxdy\int\int dx'dy'u_G^*(x,y)\\&\quad\times K^\dagger(x,y;x'',y')K(x'',y'';x',y')u_0(x',y'),\end{aligned}$$

where the Gaussian field

$$\int dx\int dyK(x,y;x'',y'')u_G(x'',y'')$$

at the mirror's location corresponds to the beam we are using to drive the cavity.

We find the result

$$\begin{aligned}\mathcal{C}=&\frac{2\pi w_0w_G}{1+iLw_G^2/2R_Gw_0^2}\\&\times\frac{\left[1-\exp\dfrac{-p^2/w_0^2(w_0^2/w_G^2+iL/2R_G)}{1+w_0^2/w_G^2+iL/2R_G}\right]}{\sqrt{\int\int dxdyu_0^2(x,y)}},\end{aligned}\tag{3}$$

whose absolute value we want to maximize. We consider the portion that depends on R_G and w_G and look for the derivative in those variables, taking into account the sign. Hence

$$\begin{aligned}|\mathcal{C}|^2\propto&\frac{w_G^2}{1+(Lw_G^2/2R_Gw_0^2)^2}\left\{\left(1-\exp\left[\frac{-(p^2/w_G^2)(1+w_0^2/w_G^2)-p^2L^2/(2R_Gw_0)^2}{(1+w_0^2/w_G^2)^2+(L/2R_G)^2}\right]\right)^2\right.\\&\left.+4\exp\left[\frac{-(p^2/w_G^2)(1+w_0^2/w_G^2)-p^2L^2/(2R_Gw_0)^2}{(1+w_0^2/w_G^2)^2+(L/2R_G)^2}\right]\sin^2\frac{p^2L/4R_Gw_0^2}{(1+w_0^2/w_G^2)^2+(L/2R_G)^2}\right\}\end{aligned}$$

has its maximum value for zero curvature, that is, $1/R_G=0$, and for w_G that solves the following equation:

$$1-\exp\left\{\frac{-(p/w_0)^2}{1+(w_G/w_0)^2}\right\}\left(1+2\frac{(w_G/w_0)^2(p/w_0)^2}{[1+(w_G/w_0)^2]^2}\right)=0.$$

B. Implications and numerical evaluation

At the input mirror

$$\sqrt[4]{\frac{2}{\pi w_G^2\,[1+(w_0/w_G)^4]}}\exp\left[-\left(\frac{1}{w_G^2[1+(w_0/w_G)^4]}+\frac{2ik}{L[1+(w_G/w_0)^4]}\right)[x^2+y^2]\right]$$

is the Gaussian beam with the largest coupling with the flat topped beam, that is, the w_G above maximizes the absolute value of Eq. (3). The main feature of the above Gaussian beam is that it resonates in a symmetric cavity and its waist is in the middle between the two mirrors. Furthermore, the scalar product

$$\mathcal{C}=\frac{2\pi w_0^2(w_G/w_0)\left(1-\exp\left\{\dfrac{-(p/w_0)^2}{1+(w_G/w_0)^2}\right\}\right)}{2\pi w_0^2\sqrt{\displaystyle\int_0^{p/w_0} r_1 dr_1\int_0^{p/w_0} r_2 dr_2\exp\{-(r_1^2+r_2^2)/2\}\mathcal{I}^0(r_1r_2)}}$$

is real. In the above equation $\mathcal{I}^0$ is the modified Bessel function of the first kind. If $\mathcal{C}$ were complex there would be a difference between the phase of the Gaussian beam that is building up power inside the resonator and the flat topped beam that is being generated by reflection of the driving beam upon the mirrors.

Also, in the Hermite-Gauss basis determined by w_G, the flat topped beam is a vector with real components.

In Fig. 6 the intensity profile of the flat topped beam is shown as a function of r/w_0 with $r=\sqrt{x^2+y^2}$. The Gaussian curve that is shown in the same graph is the one with the best coupling with the flat topped beam.

The diffraction losses are

$$\mathcal{L}_{u_G}=\int\int_{x^2+y^2\geqslant m^2}dxdy\sqrt{\frac{2}{\pi w_G^2[1+(w_0/w_G)^4]}}\times\exp\left[-\left(\frac{2(x^2+y^2)}{w_G^2[1+(w_0/w_G)^4]}\right]\right)=0.003,$$

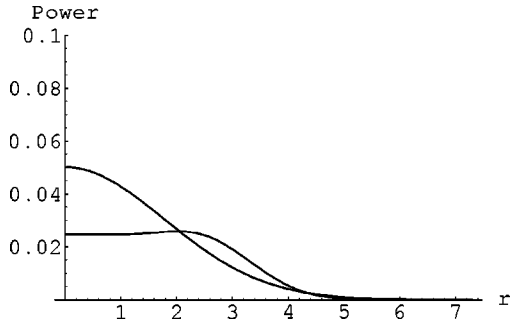

FIG. 6. The transverse power distribution of the flat topped beam and the Gaussian beam having the best coupling with it. In mirrors with diameter 32 cm the two beams have diffraction losses that are different by two orders of magnitude with smaller losses for the flat topped beam. Nonetheless, the two beams match very well. The radial variable r is expressed in units of w_0

$$\mathcal{L}_u=\frac{\displaystyle\int\int_{x^2+y^2\geqslant m^2}dxdy|u(x,y)|^2}{\displaystyle\int\int dxdy|u(x,y)|^2}=0.000021.$$

In Fig. 7 we compare the intensity of the flat topped beam with the Gaussian beam that has the same diffraction loss. In both cases we have picked $p=4w_0$, which involves $w_G=3.62w_0$ and a diameter for the mirror $2m=32$ cm.

III. ALIGNMENT STABILITY OF THE RESONATOR SUPPORTING THE FLAT TOPPED BEAM

In this section we will study the sensitivity of the electric field to a tilt of the external mirror in one cavity of the interferometer. We study spherical mirrors first for two reasons: we want to check that the results of the simulations are in agreement with the analytical predictions for the baseline design with Gaussian beams and we also want to compare the sensitivity of the flat topped beam to misalignment with that of those Gaussian beams. With spherical mirrors,

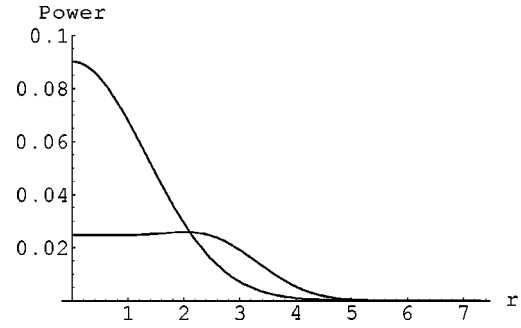

FIG. 7. The intensity of the flat topped and Gaussian beams having the same diffraction loss. The radial variable r is shown in units of w_0.

$$u_{sq}(x,y,z)=\sqrt{\frac{2}{\pi w^2(z)}}\exp\left[i\Phi_{sq}(z)-(x^2+y^2)\times\left(\frac{1}{w^2(z)}+\frac{ik}{2R(z)}\right)\right]\sqrt{\frac{1}{2^{s+q}s!q!}}H_s\times\left(\sqrt{\frac{2x}{w(z)}}\right)H_q\left(\sqrt{\frac{2y}{w(z)}}\right)$$

are the cavity modes [12].

The phase shift they acquire when propagating from one mirror to the other is

$$\Phi_{sq}(L)-\Phi_{sq}(0)=kL-(s+q+1)\times\arccos\sqrt{\left(1-\frac{L}{R(0)}\right)\left(1-\frac{L}{R(L)}\right)},$$

where $R(0)=R_1$ and $R(L)=R_2$ are the radii of curvature of the end mirrors.

We refer to the cavity in Fig. 1 for our description. If $r_2=1$ and there is no loss,

$$\psi_{in}=u_{sq}\Leftrightarrow\psi_{ref}=\frac{-r_1+e^{2i[\Phi_{sq}(L)-\Phi_{sq}(0)]}}{1-r_1e^{2i[\Phi_{sq}(L)-\Phi_{sq}(0)]}}\psi_{in}^*$$

where the coefficient in front of ψ_{in}^* is a phase factor. If L is adjusted so that $e^{2i[\Phi_{sq}(L)-\Phi_{sq}(0)]}=1$, the beam is resonating inside the cavity and

$$\psi_{ref}=\psi_{in}^*.$$

If the beam is not resonating inside the cavity, we can take the limit of high reflectivity $r_1\to 1$ and find that $\psi_{ref}=-\psi_{in}^*$. This limit can be applied only when the distinction between the resonating and the nonresonating modes is well defined; if the cavity is nearly degenerate there are quasiresonating modes in addition to the resonating one and for them the full formula for ψ_{ref} must be applied. In the LIGO the first optical modes starting from the fundamental one are nondegenerate. Since diffraction losses increase very rapidly with $s+q$, we have to consider only the low order modes.

A. Misalignment between the driving field and the axis of the cavity

We first tackle misalignment for spherical mirrors and use the basis u_{sq}.

The details of perturbation theory as applied to optical physics are given in Appendix A. At first order in the rotation angle of a mirror, the only modes that are excited are u_{10} and u_{01} if the input beam is u_{00}. When the back mirror is rotated around the y axis as in Fig. 8 the new eigenvectors of the misaligned cavity are identified using a 2×2 model:

$$v_1=\begin{pmatrix}1\\ \dfrac{ikw(L)\theta}{e^{i\eta}-e^{-i\eta}},\end{pmatrix}=v_1^*,\quad v_2=\begin{pmatrix}\dfrac{ikw(L)\theta}{e^{-i\eta}-e^{i\eta}}\\ 1\end{pmatrix}=v_2^*,$$

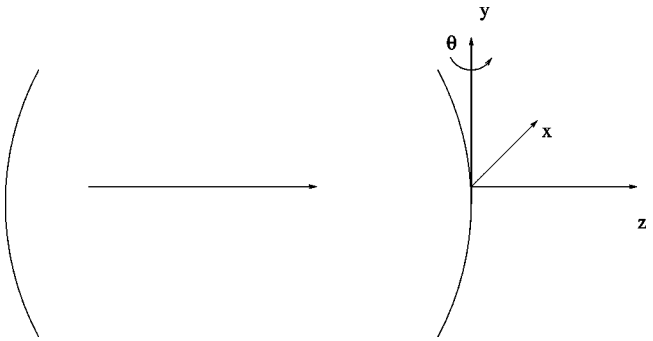

FIG. 8. If one mirror is rotated by θ around the $\hat{y}$ axis, its surface is displaced by an amount $\delta z(x,y)=-\theta x$, where z has the same direction as the incoming beam. Similarly, if it is rotated by θ around $\hat{x}$ the surface of the mirror is moved by $\delta z(x,y)=\theta y$.

where $\eta=\Phi_{10}(L)-\Phi_{10}(0)-\Phi_{00}(L)+\Phi_{00}(0)$. The notation we are using is

$$u_{00}=\begin{pmatrix}1\\0\end{pmatrix},\quad u_{10}=\begin{pmatrix}0\\1\end{pmatrix}.$$

The input field is

$$u_{00}=v_1-\frac{ikw(L)\theta}{e^{i\eta}-e^{-i\eta}}v_2.$$

If the cavity is properly tuned to make v_1 resonate, the reflected field is

$$v_1+\frac{ikw(L)\theta}{e^{i\eta}-e^{-i\eta}}v_2=\begin{pmatrix}1\\ \dfrac{2ikw(L)\theta}{e^{i\eta}-e^{-i\eta}}\end{pmatrix}.$$

In the whole interferometer the symmetric combination of the fields reflected from the two arms goes through the symmetric port of the beam splitter and the antisymmetric combination exits through the dark port. If only one of the two arms is misaligned in the way described above, the ratio of the dark port to the bright port power,

$$\frac{P_{DP}}{P_{BP}}=\left(\frac{kw(L)\theta}{2\sin\eta}\right)^2=0.2192\left(\frac{\theta}{\mu\,\mathrm{rad}}\right)^2,$$

is predicted according to the design parameters of the advanced LIGO, which include $k=2\pi/\lambda$ with $\lambda=1.064\ \mu$m and $R(0)=R(L)=54$ km. The length of the Fabry-Pérot arm is $L=3999.01$ m and these are the same parameters we have used for estimating the diffraction losses in Sec. I. From the numerical simulations we have obtained the data shown in Fig. 9, which are best fitted by the curve

$$\frac{P_{DP}}{P_{BP}}=0.2196\left(\frac{\theta}{\mu\,\mathrm{rad}}\right)^2$$

with an agreement of $\sim 0.2\%$ with the theoretical estimation. The analysis we have done so far can be repeated if the front mirror of a cavity is tilted.

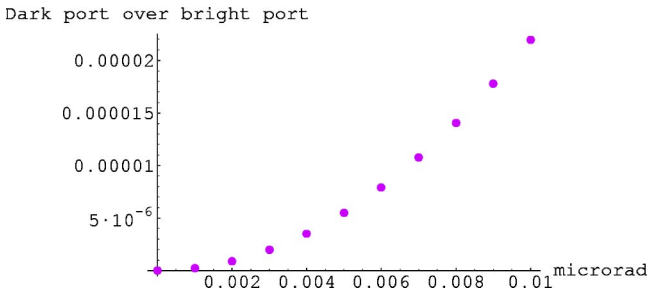

FIG. 9. The ratio of the dark port to the bright port is reported as a function of the angle error for the back mirror of one arm according to the parameters of the advanced LIGO.

B. Investigation of the effects of misalignment for flat topped beam

For our initial studies we have decided not to implement the recycling mirror in Fig. 2. In practice we had to set $r_r = 0.000015$ in order to make the code work. The FFT model that we have used sets the length of each cavity by maximizing the circulating power of the electric field. The two Fabry-Pérot arms are pseudolocked first and then the recycling cavity: the distance between the end mirrors in each cavity is adjusted in order to make the circulating field resonate. This procedure is repeated until stationarity is achieved, which means the power levels and the round-trip phases do not change from one iteration to the next by more than a certain threshold which is decided by the user. Since any round-trip phase is computed by making the field propagate and be bounced from the optics, none of the mirrors can be absent, otherwise the code fails to converge. Although the recycling mirror cannot be removed its reflectivity can be very small. We used the parameters $t_2 = 0$ and $t_1 = \sqrt{0.005}$ which we had chosen for testing spherical mirrors. We checked that the phase of the field matches the surface of the mirrors when stationarity is achieved. If

$$\mathcal{C} = 0.97, \quad \mathcal{L}_u = 0.000021,$$

as we have estimated, when P_0 is the amount of power input to the system

$$\frac{P_{cav}}{P_0} = \frac{1}{2}|\mathcal{C}|^2 \frac{t_r^2}{(1-r_r)^2} \frac{t_1^2}{(1-\sqrt{1-t_1^2-\mathcal{L}_u}\sqrt{1-\mathcal{L}_u})^2} = 372, \tag{4}$$

and the numerical result

$$\frac{P_{cav}}{P_0} = 373$$

is very close to the prediction. We also looked at the data for the total loss

$$\frac{P_0 - P_{out}}{P_0} = \frac{P_0 - P_{DP} - P_{refl}}{P_0} = 0.028,$$

where P_{refl} is the power reflected back toward the laser. The diffraction loss that we infer,

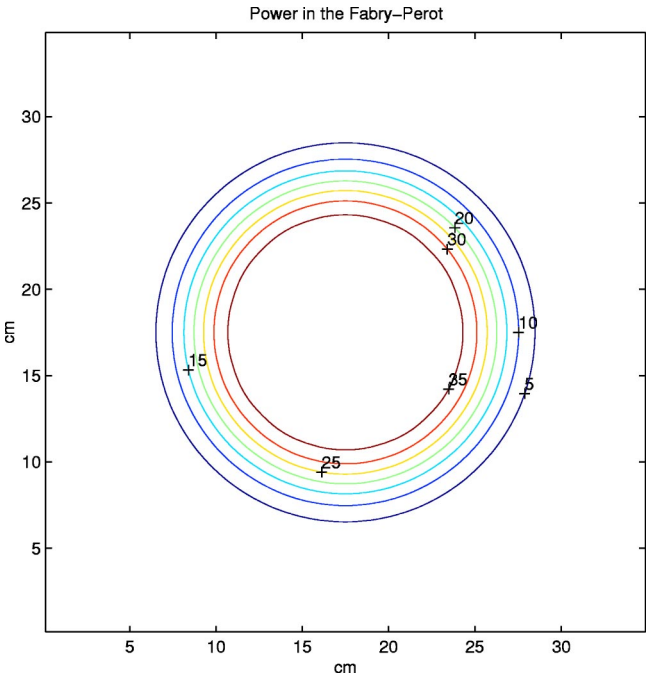

FIG. 10. The intensity profile of the beam resonating in a cavity with nonspherical mirrors which are designed to make the built-up field very flat.

$$0.028 = 4\frac{P_{cav}}{P_0}\mathcal{L}_u \Rightarrow \mathcal{L}_u = 0.000019,$$

substituted in Eq. (4), gives $P_{cav}/P_0 = 373$. This may suggest that the finite size of the mirrors makes the shape of the field change, so that if we use the ideal beam in our formula the result is slightly off. The intensity of the beam as computed by postprocessing the data obtained by the numerical simulations is shown in Fig. 10. When one mirror is tilted we want to repeat the analysis we have done for spherical mirrors. Although we do not know the higher order modes, we can use symmetry properties to infer that the first excited component will be odd in x for rotations around $\hat{y}$. Using this feature we quantified the impact of misalignment on the flat topped beam.

Since we know the shape of the beam in the unperturbed case, we can project the field resonating in the misaligned cavity onto that and remove that part. What is left is divided into an odd and an even component in x. If the perturbation is small the odd part is proportional to θ and the even part proportional to θ^2. The power associated with those two components has been evaluated for 11 runs, with $0 \leqslant \theta \leqslant 10^{-8}$ rad. In Fig. 11 and Fig. 12 the intensities of the excited odd and even contributions are shown. By fitting the data, we can evaluate the coefficients for the first terms in the expansion of the eigenvector resonating inside the misaligned cavity. Since our analysis is based on the electric field picked up at the front mirror, which is unperturbed, the eigenvector must be real in the basis of the unperturbed eigenvectors. The data are fitted by

$$v_{tilt} = \alpha_0 u + \alpha_1 u_{odd} + \alpha_2 u_{even},$$

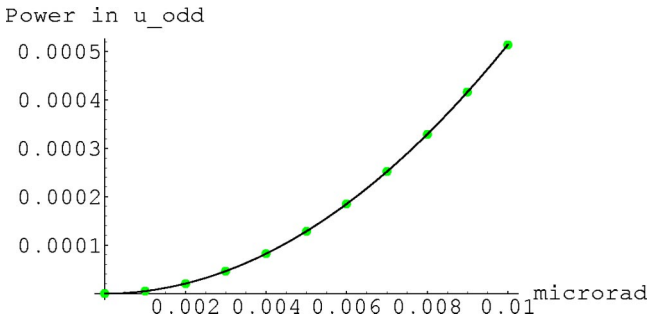

FIG. 11. Results of the evaluation of the portion of power due to tilt at the first order in the angle error. This is the main contribution to higher order modes when the cavity is misaligned, thus generating a signal out of the dark port because this perturbation breaks the symmetry of the interferometer.

$$\alpha_0^2 = \frac{P_u}{P_{tot}} = 1 - \alpha_1^2 - \alpha_2^2,$$

$$\alpha_1^2 = \frac{P_{odd}}{P_{tot}} = 5.1426\left(\frac{\theta}{\mu\,\mathrm{rad}}\right)^2,$$

$$\alpha_2^2 = \frac{P_{even}}{P_{tot}} = 4.12\left(\frac{\theta}{\mu\,\mathrm{rad}}\right)^4,$$

and we can use the above information to interpret the signal at the dark port of the interferometer. We compute the fraction of input power that goes out of the dark port because of the misalignment of one of the two long arm cavities:

$$\frac{P_{DP}}{P_0} = |\mathcal{C}|^2\alpha_1^2 = 4.84\left(\frac{\theta}{\mu\mathrm{rad}}\right)^2, \tag{5}$$

and the numerical result

$$\frac{P_{DP}}{P_0} = 4.82\left(\frac{\theta}{\mu\mathrm{rad}}\right)^2$$

is close to Eq. (5) within 0.4% (see Fig. 13). As for the spherical mirrors case, if the odd component were filtered out, the signal at the dark port would be much decreased. In Fig. 14 the power at the dark port is shown as a result of a

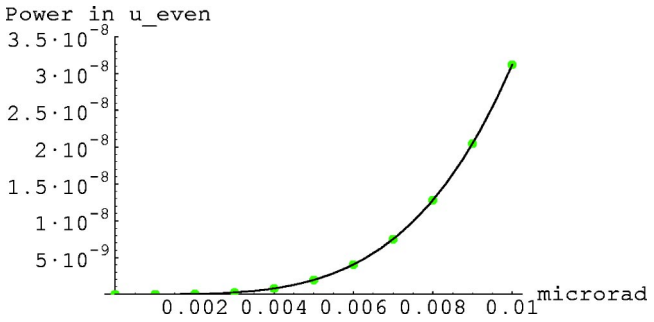

FIG. 12. The modes that are excited at second order when one mirror is tilted do not contribute much if the angle is not larger than 10^{-8} rad.

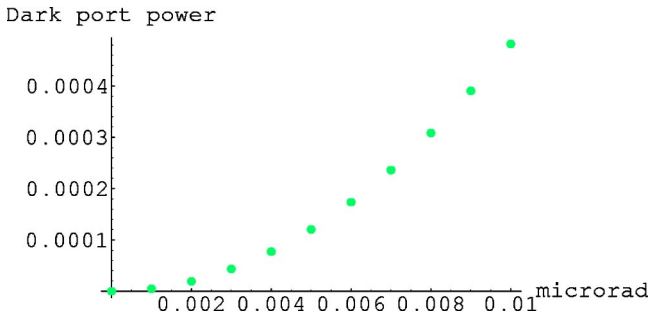

FIG. 13. When one mirror is misaligned, the power exiting the dark port is quadratic in the tilt angle. The excited field is odd in x for a rotation around $\hat{y}$ and odd in y for a rotation around $\hat{x}$. The physical mechanism is the same as in the more common case of tilt in spherical mirrors.

total suppression of the odd contribution. The best fit for those data is

$$\frac{P_{DP}^{nondip}}{P_0} = 31.5\left(\frac{\theta}{\mu\mathrm{rad}}\right)^4,$$

which is comparable with

$$\frac{P_{DP}^{nondip}}{P_0} = |\mathcal{C}|^2(\alpha_1^4 + \alpha_2^2) = 28.8\left(\frac{\theta}{\mu\mathrm{rad}}\right)^4.$$

The intensity of u_{odd} is shown in Fig. 15. The excited component has the very topology we expect from geometrical considerations. Although this is what could have been inferred by analogy with spherical mirrors, we found a quantitative relationship between the misalignment and the variation of the beam. When the second order perturbation is taken into account, the change in the surface of the mirror due to the orientation has a more general effect: not only is there a new axis of the cavity but the phase profile sensed by the beam is quite different. In Fig. 16 the power associated with u_{even} has a very peculiar distribution: the analogy with spherical mirrors is broken since when the beam does not impinge on the center of the reflecting surface, the shape of the sensed reflecting surface is different from the unperturbed situation. For spherical mirrors this is not the case,

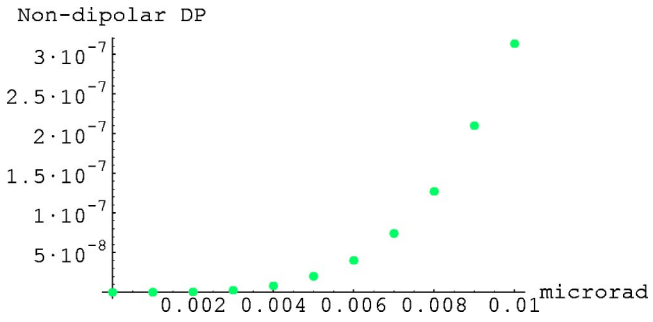

FIG. 14. The field at the dark port due to small misalignments consists of the antisymmetric combination of the beams coming from the two cavities. A small portion corresponds to the unperturbed mode and that is due to slightly different reflectivities when the field is bounced back from the two cavities.

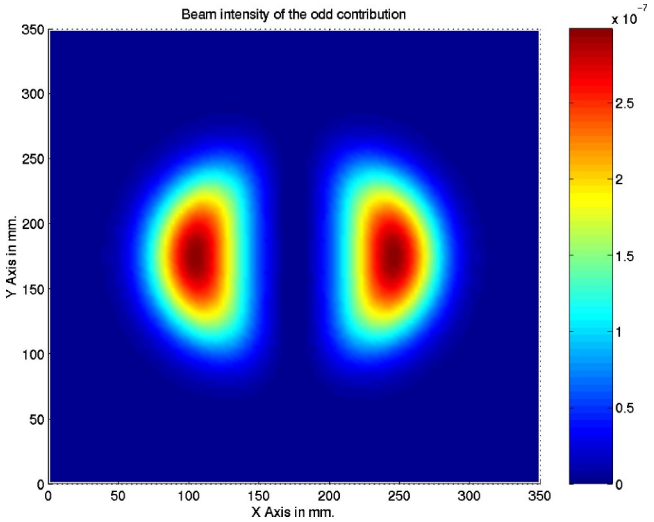

FIG. 15. The variation of the resonating electric field due to a small misalignment of one mirror is proportional to the angle error and is odd with respect to the axis of rotation. We have named such variation u_{odd} and it has been extracted from the grid representing the transverse amplitude of the field, obtained by simulations.

since they have the same curvature for any point on their surface the beam happens to hit. In Fig. 16 we see a quadrupole form intensity.

Since the shape of the beam is affected, the thermoelastic noise integral that corresponds to the field circulating in the misaligned cavity is also changed [6].

The results obtained by O'Shaughnessy set a requirement for the angle error. He and Strigin have calculated the excitation of the mirrors due to thermoelastic interaction with the beam for different configurations. There are options that involve reshaping the bulk of the mirrors, which allows a large reduction of thermoelastic noise [6].

A mode cleaner introduced at the output of the interferometer can be used for filtering out the main contribution (5)

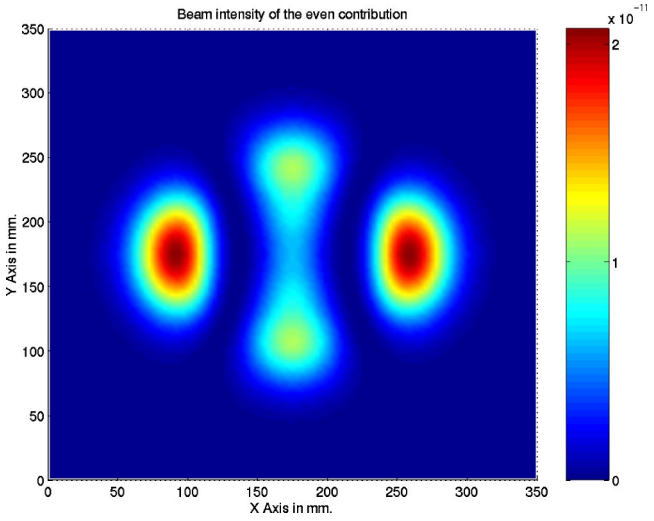

FIG. 16. The second order perturbation of the resonating field is small and looks like a quadrupole; since the mirror is nonspherical a tilt involves a change of the symmetry of the beam that goes beyond the simple variation of the direction of propagation.

at the dark port. The design for this mode cleaner is similar to the Fabry-Pérot cavity of Fig. 1. If we take $r_1=r_2$ all the light of the resonating mode is transmitted. The higher order modes are suppressed:

$$\frac{|\psi_{tr}|^2}{|\psi_{in}|^2}=\frac{t_1^2t_2^2}{(1-r_1r_2)^2[1+(4r_1r_2\sin^2\overline{\eta})/(1-r_1r_2)^2]}$$

when the round-trip phase $2\overline{\eta}\gg(1-r_1r_2)$. Compared to the fundamental mode we have a reduction $\sim 4r_1r_2\sin^2\overline{\eta}/(1-r_1r_2)^2$. This factor can be very high.[1]

There is one more detail to be investigated, which is how misalignment modifies diffraction losses. We studied the interaction of a beam representing the fundamental mode of the unperturbed cavity with the misaligned cavity. We found that when the cavity is not driven by a cavity mode, there is a mismatch at the input mirror, and because of that only a fraction of the input power is available to be stored in the resonating mode. This makes the power level drop down in the resonator.

We therefore analyze how diffraction depends on the tilt angle, since this can cause the power gain to decrease. Since the variation should be $\sim\theta^2$,

$$L_{v_{tilt}}=L_u+\alpha_1^2(L_{u_{odd}}-L_u)+\int\int_{x^2+y^2>m^2}dxdy2\Re[\alpha_2u^*(x,y)u_{even}(x,y)],$$

we expect a small impact on the total power reflected back from the cavity. If there is any difference in the reflectivities from the two arms, the result is a deteriorated contrast, with some light exiting the dark port. By fitting the data for the total power lost because of increased diffraction losses, we find

$$\delta r_{eff}=-0.51\left(\frac{\theta}{\mu\text{rad}}\right)^2,$$

and on adding the term

$$|\mathcal{C}|^2\left(-\delta r_{eff}\alpha_1^2+\frac{\delta r_{eff}^2}{4}\right)=2.5\left(\frac{\theta}{\mu\text{rad}}\right)^4$$

to our first estimation above we obtain a value close to the numerical result for P_{DP}^{nondip}/P_0 within a few percent. All these runs and checks with analytical predictions make us confident of the analogy between the behavior of the flat topped beam and the more common Gaussian beams. The characteristic shape of u_{odd}, for example, makes it suitable for the control system. Since the intensity is shifted from the unperturbed axis when there is misalignment, the same method used to correct the angular displacement of spherical mirrors will work for flat topped beams. If the light distribu-

[1]In order to recover a better shot-noise sensitivity, VIRGO decided to use an output mode cleaner to reduce the contrast defect [13].

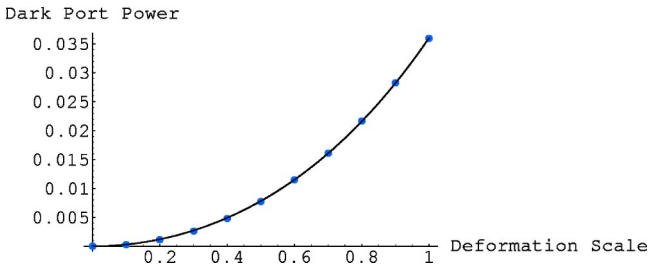

FIG. 17. We have introduced one realistic mirror in the interferometer. The imperfections have been scaled down by the factor shown on the horizontal axis and the corresponding power at the dark port is reported on the vertical axis. If all the mirrors are affected by a similar deformation the power which is lost through the excitation of higher order modes is four times the values shown in this graph.

tion is not symmetric in two half planes of the photodetector used in the control system, the alignment is to be corrected [14,15].

IV. SENSITIVITY OF THE FLAT TOPPED BEAM TO REALISTIC SURFACE DISTORTIONS

We want to analyze the impact of mirror imperfections on the profile of the beam. Any advantage obtained by using a field with flat intensity distribution would be lost if the shape of the beam were completely changed because of any distortion in the mirror surfaces. In order to study a realistic situation we used the measurements of the surface of a LIGO I beam splitter, because that is the flattest mirror we currently have that satisfies the requirements of the LIGO.[2]

A map of the deformations was provided by Garilynn Billingsley of LIGO Laboratories. In this section we report and comment on our study of the influence of realistic figure errors for the mirrors on the interferometer's perfomance.

Although the deformation can be considered realistic, Billingsley told us that mirrors can be manufactured much more accurately. Hence we have regarded it as the most pessimistic case.

We scaled down the data of the distortion and put the manipulated map of deviations from flatness on the top of the external mirror in one Fabry-Pérot cavity of the interferometer.

As we learnt from analyzing misalignment, if only one cavity is perturbed the signal at the dark port is generated by the higher order modes excited by the distortion. In Fig. 17 the power at the dark port versus the size of the imperfections is shown. The scale factor in front of the deformation is $\epsilon \in [0,1]$. The best fit for the numerical data is the following curve:

$$\frac{P_{DP}}{P_0} = 0.0297\epsilon^2 + 0.0064\epsilon^4.$$

[2]For an exhaustive overview of metrology procedures, see [16].

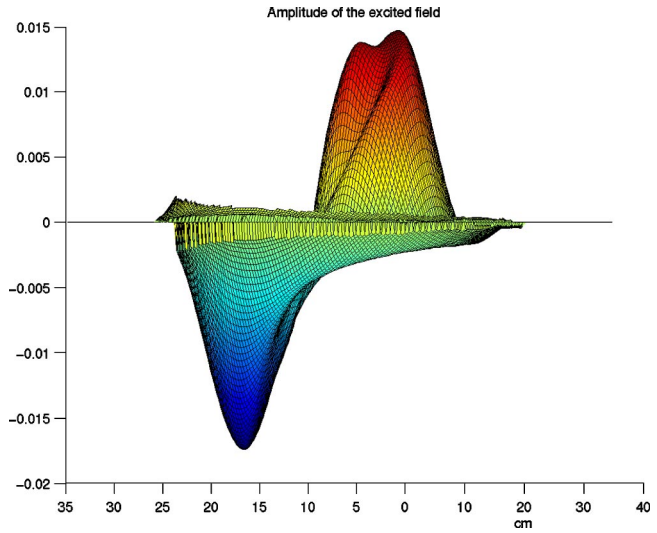

FIG. 18. This is the change in the shape of the resonating beam due to realistic mirrors obtained by overlapping the perfect mirror with the typical deviations we might expect.

With a view to restricting our analysis to a regime of linearity, we have decided to choose $\epsilon = 0.2$. For larger values $\epsilon \geqslant 0.4$ the influence of the tilt on the interferometer's performance computed by analysis of the data obtained by the FFT model and the predictions based on the perturbative model O'Shaughnessy has implemented are in disagreement, although several modes have been used, while the agreement is excellent for the value $\epsilon = 0.2$, which Billingsley believes should be achievable by mirror manufacturers, at least in the innermost 10 cm (the area that is most important for its influence on the impinging field), by coating.

We set $\epsilon = 0.2$ and for this value 99% of the power at the dark port is proportional to $\sim \epsilon^2$. The resulting change in the beam contains a large component of odd modes as is shown in Fig. 18. We used a procedure similar to the one set up for studying the influence of tilt on the resonating beam, in order to identify the perturbed cavity mode and express it as a combination of the unperturbed cavity modes. Using a formalism similar to the one introduced above,

$$v_{def} = \alpha_0 u + \alpha_{exc} u_{exc}$$

is the field resonating inside the cavity with a perturbed external mirror. It can be expressed as its projection upon the unperturbed flat topped beam plus the remaining excited component.

Then we can look for the odd contributions. We use the results obtained by our simulations for misalignment to estimate the angle error corresponding to the dipolar component of the excited field. We expect that adjusting the alignment of the mirror can reduce the impact of the fabrication imperfections. When a significant amount of the dipolar field is minimized by realigning the mirror, the output power is reduced:

$$\frac{P_{DP}}{P_0} = 0.38 \times 10^{-3},$$

while without the proper adjustment the dark port power is three times larger:

$$\frac{P_{DP}}{P_0} = 1.13 \times 10^{-3}.$$

This test shows again that the flat topped beam behaves similarly to the much more common Gaussian beams.

If the mirror distortions are not axially symmetric, the light distribution is slightly off center on the transverse plane. The control system which measures and compares the intensity of the electric field in two half planes separated by the $\hat{y}$ and $\hat{x}$ axes will partly compensate for the perturbation [17].

Also, in order to have small variations in the linear regime the distortion in the central area must be less than 6 nm. The phase change sensed by the electric field,

$$\int \int_{x^2+y^2 \leq m^2} dxdy u^*(x,y) \exp[2ik\Delta z(x,y)] u(x,y),$$

must be much smaller than the phase difference between the optical modes. When this is not the case the higher order modes are easily excited and the cavity is no longer supporting the flat topped beam. For this reason, any perturbation that contains a tilt effect can greatly affect the shape of the beam, since it couples the fundamental mode with the first excited mode. The angle error will be detected by the control system, which is aimed to minimize the asymmetry in the power distribution of v_{def}. The difference in the overlap between u and v_{def} over two half planes is computed through a quadrant diode; it is the error signal that is fed back to the perturbed mirror to control its tilt.

We made one more test that also helps in understanding the importance of a smooth profile in the central area; we scaled the realistic deformation down by the factor $\epsilon = 0.2$ only in the central area. On the rim we kept the entire value. We found the result

$$\frac{P_{DP}}{P_0} = 3.02 \times 10^{-3},$$

which is three times larger than the value obtained by scaling down the whole realistic deformation and more than ten times smaller than the value obtained by using the whole realistic deformation. In Fig. 19 the data we used scaled down by $\epsilon = 0.2$ are shown. The modified version is shown in Fig. 20. In the latter, the measured data for the deformation have been multipled by 0.2 for $r \leq 9.6$ cm. In the outer region $r \geq 12.2$ cm we kept the measured values, and in between we linearly interpolated to make the transition smooth.

Some crucial issues related to the design of the recycling cavity

The main source of diffraction loss in LIGO consists of the beam splitter, which faces the circulating field at 45°. If we take a beam splitter with the same diameter as the mirrors,

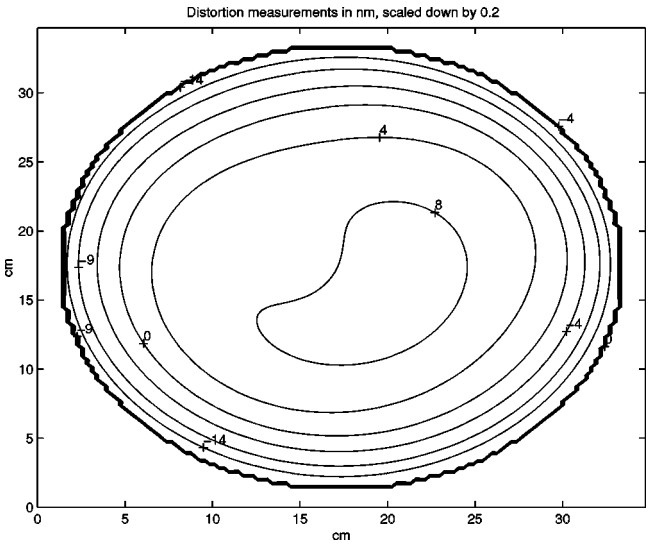

FIG. 19. The features of the deformation we have used are shown in this figure, which is obtained by scaling the measured values by $\epsilon = 0.2$. The profile of the mirror is changed by $\sim 20 - 30$ nm in the outer region. The asymmetry in the central area has an effect equivalent to misalignment; if the mirror is slightly tilted in order to compensate for that, the power at the dark port is noticeably decreased. This power is due to the higher order modes excited in the cavity, whose external mirror is affected by the deformation shown in this map.

$$\mathcal{L}_u^{BS} = \frac{\int \int_{2x^2+y^2 \geq m^2} dxdy |u(x,y)|^2}{\int \int dxdy |u(x,y)|^2} = 0.00834$$

in the clipping approximation.

For such diffraction loss,

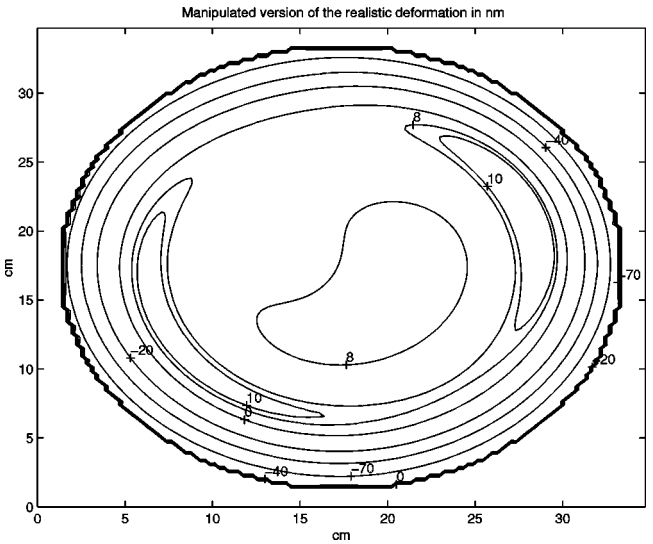

FIG. 20. This figure represents the manipulation of the realistic deformation we did by scaling down the data for the central area, keeping the rim as it is from measurements.

$$\frac{P_{cav}}{P_0}=|\mathcal{C}|^2\frac{1-\mathcal{L}_u^{BS}}{2}\frac{t_r^2}{(1-r_{eff}\sqrt{1-t_r^2-\mathcal{L}_u})^2}\times\frac{t_1^2}{(1-\sqrt{1-t_1^2-\mathcal{L}_u}\sqrt{1-\mathcal{L}_u})^2}=7822,$$

$$\frac{P_{RM}}{P_0}=|\mathcal{C}|^2\frac{t_r^2}{(1-r_{eff}\sqrt{1-t_r^2-\mathcal{L}_u})^2}=20.07 \quad \text{at the recycling mirror,}$$

$$\frac{P_{BP}}{P_0}=|\mathcal{C}|^2\frac{t_r^2 r_{eff}^2}{(1-r_{eff}\sqrt{1-t_r^2-\mathcal{L}_u})^2}=19.15 \quad \text{at the bright port,}$$

where we have defined

$$r_{eff}=\frac{1-\mathcal{L}_u^{BS}}{2}\frac{-r_1+r_2}{(1-\sqrt{1-t_1^2-\mathcal{L}_u}\sqrt{1-\mathcal{L}_u})^2} \tag{6}$$

and used our result $\mathcal{L}_u=0.000019$ as obtained in Sec. III. If we compare the above predictions with the numerical outcome of the simulation,

$$\frac{P_{cav}}{P_0}=5958,$$

$$\frac{P_{RM}}{P_0}=15.28,$$

$$\frac{P_{BP}}{P_0}=14.35,$$

we find a large discrepancy due to the underestimation of $\mathcal{L}_u^{BS}$.

Therefore we compute the total loss, from which we can infer how much light is diffracted away through the beam splitter. In Sec. III $\mathcal{L}_u$ was estimated by the same method and the numerical and analytical results were not exactly the same. Using the numerical estimation for $\mathcal{L}_u$, we calculate

$$\frac{P_0-P_{refl}-P_{DP}-4P_{cav}\mathcal{L}_u-P_{RM}\mathcal{L}_u-P_{BP}\mathcal{L}_u}{P_0(P_{RM}+P_{BP})}=\mathcal{L}_u^{BS}=0.0162 \tag{7}$$

and in fact inserting this value in our analytical formulas gives the correct predictions within 0.8%. We used $t_r=\sqrt{0.06}$ because this is the transmittivity of the recycling mirror required for the next configuration of the LIGO. The other values are $t_1=\sqrt{0.005}$ and $t_2=0$, and any reflectivity is defined such that

$$t_1^2+r_1^2+\mathcal{L}_u=t_2^2+r_2^2+\mathcal{L}_u=t_r^2+r_r^2+\mathcal{L}_u$$

is always applied. Since $r_{eff}<1$ because of the losses in Eq. (6), if we compute the power carried by the field that exits the bright port and goes toward the recycling mirror and the power carried by the field that is going from the recycling mirror toward the beam splitter, we find a small difference.

The beam splitter needs to be fabricated larger to reduce the diffraction loss, or other means need to be applied. For example, the bulk of the internal test mass mirrors that are the input mirrors of the two arm cavities can be designed in order to make the beam converge toward a closest focus. The thermoelastic noise depends on the intensity of the beam; the power circulating in the Fabry-Pérot cavities is about 400 times larger than in the recycling cavity. This allows less strict requirements for the design of the recycling cavity. We can even afford conical shape mirrors for the internal test masses, which will further reduce the thermoelastic noise. In principle, the recycling cavity can be affected by losses that are two orders of magnitude larger than in the arm cavities. For example, the diffraction loss (7) must be reduced by at least one order of magnitude but it does not need to be $\sim\mathcal{L}_u$. There are also motivations for allowing the beam not to be flat in the recycling cavity, related to the quasidegeneracy that affects the sidebands. They contribute to both the control and the detection scheme. The sidebands circulate only in the recycling cavity and the higher order modes are easily excited, because of the small difference between the eigenvalues of the round-trip propagator. We found, for example, that the sensitivity of the beam to imperfections affecting the mirror surfaces is one order of magnitude larger in the recycling cavity than in the Fabry-Pérot cavity. This would put tight requirements on the surface of the mirrors that are comparable with the accuracy of the data we have used for the typical distortions.

V. SUMMARY AND REMARKS

After thermoelastic noise was found to be the dominating problem for the advanced LIGO, to reach the sensitivity level due to the quantum noise limit much study and reasearch has been done by a collaboration led by Thorne. Since the reduction of thermoelastic noise has been shown to be significant by using mirrors with a special shape, some fundamental issues related to the implementation of those mirrors have been examined by both simulations and analytical calculations.

Several FORTRAN programs were written for analyzing the maps of the beam inside the interferometer and at the external pickup points to study how the field is affected by realistic perturbations. We processed the results in order to quantify the impact of misalignment on the flat topped beam. The data were compared with the same effect concerning the advanced LIGO. Our analysis shows that the tilt angle must be controlled $\sim$five times better. The current fluctuations are $\sim 10^{-8}$ rad with a spectrum decreasing as $\sim f^{-1}$.

We also showed that the most important excited contribution is dipolar (Fig. 13) so that it can be filtered out by using a mode cleaner. Since the excited field has the same geo-

metrical asymmetry around the rotation axis of the tilted mirror, the physical principles and the control system that work for the Gaussian beams apply to the flat topped beam as well. We reviewed the mirrors that support the flat topped beam and studied how deviations from the ideal surface can modify its shape. In Fig. 17 the power that is transferred to higher order modes and thus exits the dark port depends on the size of the typical deformations of one mirror. If all mirrors are affected by similar uncorrelated distortions, we expect four times that amount, which means

$$\frac{P_{DP}}{P_0} \in [0.005,0.01] \Rightarrow \max[\Delta z(x,y)] \in [4 \text{ nm},6 \text{ nm}] \quad (8)$$

in the central area.

Furthermore, if the real mirrors are affected by a large nonaxially symmetric perturbation the alignment can be corrected to partially compensate for it. In the specific case we analyzed, we found an impact on the flat topped beam equivalent to a tilt of

$$\theta = 0.013 \ \ \mu \text{ rad}$$

of the mirror around the axis at $-55°$ in its $\hat{x},\hat{y}$ plane. Since the control system measures the asymmetry of the intensity in two half planes, this correction is feasible.

The requirements in Eq. (8) are imposed by the limits due to shot noise [18]. The shot noise increases with $\sim \sqrt{P_{DP}}$. The sidebands contribute to shot noise even when the interferometer is perfect, since they are transmitted through the dark port with almost their total power. If higher order modes are excited, less power is available in a suitable form for signal detection and the excess power contributes to shot noise. We simulated the whole system with the recycling cavity included, to study the impact of mirror deformations on the circulating field.

From the results of this last set of simulations, having the same requirements for P_{DP}/P_0 as in Eq. (8) implies $\max[\Delta z(x,y)] \sim 1$ nm. This constraint is of the same order of magnitude as the accuracy of the data that have been the basis for our numerical investigations of the mirror's deformations.

With the current technology, mirrors whose central region has a peak-to-valley error of the order of ~ 5 nm are attainable according to Billingsley. Every requirement first entails investigations of its feasibility. Because of its short length the recycling cavity is deeply affected by any distortion in the mirror profiles. The results of our simulations suggest that the field need not be flat in the recycling cavity and is matched through a lens to the flat topped beam resonating in the Fabry-Pérot cavity where thermoelastic noise dominates.

Several options have been studied although we have presented here one typical case. Both the size of the reflecting surface and the shape of the mirrors are variables that can be properly designed to further reduce thermoelastic noise.

When the constraints on the fabrication of large crystals of sapphire are exhaustively understood the optimal choice can be selected among many options [6].

A quantitive analysis of thermoelastic noise has been done by O'Shaughnessy, Strigin, and Vyatchanin using a finite element model program. Although their results required sophisticated computations, a rough estimation can be done easily for the reduction of thermoelastic noise (through a flat topped beam instead of a Gaussian one) that is based on a comparison between the beam we have chosen to drive the Fabry-Pérot cavity (by optimizing its overlap with the flat topped beam) and the Gaussian beam characterized by the advanced LIGO baseline design. We find

$$\frac{S_{flattop}}{S_{LIGO\ II}} = \left(\frac{w}{w_G}\right)^3 \simeq (6 \ \text{cm}/9 \ \text{cm})^3 = 0.3$$

by simply applying the scaling law $\sim w^{-3}$ for thermoelastic noise. This estimate is very close to the numerical result reported in [6] for the specific case we have analyzed in this paper. This estimation implies that the sensitivity of the advanced LIGO with a flat topped beam will improve up to the limit due to quantum noise. Further reduction can be obtained by reshaping the bulk of the mirrors [6].

ACKNOWLEDGMENTS

I would like to thank Kip S. Thorne for introducing me to this research issue. I owe a lot to Kip and William Kells, for they have been generous in ideas and suggestions. A great deal of gratitude is also due to Stanley Whitcomb because I never lacked his encouragement. Richard O'Shaughnessy and I had many discussions; thanks to the effort of both we found valuable results. One of the simulation tools we used is a FORTRAN program that has had interesting applications in modeling optical imperfections. That code has been very useful in simulating the interferometer and several scientists of the LIGO community have contributed to its development. We acknowledge Brett Bochner and Yaron Hefetz. The other numerical tool we used is a steady-state analytical model, whose aim is to expand the electromagnetic field everywhere in the interferometer, using a set of unperturbed spatial basis functions. This model is widely employed by the LIGO community and its development is fundamentally due to Ray Beausoleil *et al.* [19]. We are grateful to the Center for Advanced Computing Research whose computers we have been using. This research was supported by the National Science Foundation under Cooperative Agreement No. PHY-9210038 and the California Institute of Technology.

APPENDIX A: PERTURBATION THEORY APPLIED TO EVALUATE THE EFFECTS OF MISALIGNMENTS

First of all let us define the eigenvectors for the operator that represents a round-trip propagation inside a cavity, with spherical mirrors whose curvature is R_1 and R_2,

$$\hat{L}(\vec{r_f},\vec{r_i},0) = \int\int d^2\vec{r} e^{-ik|\vec{r_f}|^2/R_1} \frac{k}{2\pi iL} e^{ik[L+|\vec{r_f}-\vec{r}|^2/2L]} \times e^{-ik|\vec{r}|^2/R_2} \frac{k}{2\pi iL} e^{ik[L+|\vec{r}-\vec{r_i}|^2/2L]},$$

where $\vec{r}_i$ and $\vec{r}_f$ are the initial and final transverse positions. Since the above operator is not Hermitian, there is a set of left and a set of right eigenvectors. We can use the biorthogonality between these two sets with a view to the application of the techniques of perturbation theory to problems connected with deformations which induce a variation in the circulating field:

$$(\hat{L}+\hat{L}_{pert})\left(|u_n\rangle+\sum_{n'} C_{n'}^{(n)}|u_{n'}\rangle\right)$$

$$=(\lambda_n+\Delta\lambda_n)\left(|u_n\rangle+\sum_{n'} C_{n'}^{(n)}|u_{n'}\rangle\right)$$

$$\langle\tilde{u}_n|\hat{L}_{pert}|u_n\rangle=\Delta\lambda_n,$$

$$\langle\tilde{u}_{n'}|\hat{L}_{pert}|u_n\rangle=(\lambda_n-\lambda_{n'})C_{n'}^{(n)},$$

where we have defined

$$\hat{L}|u_n\rangle=\lambda_n|u_n\rangle,\quad \langle\tilde{u}_n|\hat{L}=\langle\tilde{u}_n|\lambda_n$$

$$\langle\tilde{u}_n|u_m\rangle=\delta_{nm}.$$

We can apply the above formalism to some typical perturbation. For example, when a variation of the radius of curvature of the back mirror occurs, the surface of the mirror is displaced by the amount $\Delta z(\vec{r},L)$, giving the result

$$C_{n'}^{(n)}=\frac{\lambda_{n'}^{1/2}\lambda_n^{1/2}}{\lambda_n-\lambda_{n'}}\int\int d^2\vec{r}\tilde{u}_{n'}^*(\vec{r},L)[e^{2ik\Delta z(\vec{r},L)}-1]u_n(\vec{r},L),$$

$$C_{20}^{(00)}=C_{02}^{(00)}=\frac{e^{3i\eta}e^{i\eta}}{e^{2i\eta}-e^{6i\eta}}\left[-\frac{ikw(L)^2}{2\sqrt{2}\left(\frac{1}{R_{pert}}-\frac{1}{R_2}\right)}\right].$$

For a rotation θ of the back mirror around the $\hat{y}$ axis, the above formalism gives the correction

$$C_{10}^{(00)}=\frac{e^{2i\eta}e^{i\eta}}{e^{2i\eta}-e^{4i\eta}}[-ikw(L)\theta]$$

with the following eigenvectors:

$$u_n=u_{sq}(x,y,z)$$
$$=\sqrt{\frac{2}{\pi w^2(z)}}\exp\left[i\Phi_{sq}(z)-(x^2+y^2)\times\left(\frac{1}{w^2(z)}+\frac{ik}{2R(z)}\right)\right]\sqrt{\frac{1}{2^{s+q}s!q!}}\times H_s\left(\sqrt{\frac{2x}{w(z)}}\right)H_q\left(\sqrt{\frac{2y}{w(z)}}\right) \quad \text{(A1)}$$

for the unperturbed state.

The corresponding eigenvalues are

$$\exp\{2i[\Phi_{sq}(L)-\Phi_{sq}(0)]\}=\exp\left[2ikL-2i(s+q+1)\times\arccos\sqrt{\left(1-\frac{L}{R_1}\right)\left(1-\frac{L}{R_2}\right)}\right] \quad \text{(A2)}$$

for a round-trip propagation. Our reference for the expansion is Eq. (A1) defined at $z=0$. This choice implies that the eigenvectors of the perturbed cavity have the same wave front as the unperturbed eigenvectors at $z=0$ if the input mirror is not distorted.

When the input mirror is tilted by θ' around the $\hat{y}$ axis, we have

$$C_{10}^{(00)}=\frac{e^{4i\eta}}{e^{2i\eta}-e^{4i\eta}}[-ikw(0)\theta'],$$

where we have used

$$e^{i(s+q)\eta}=\exp\{[i(\Phi_{sq}(L)-\Phi_{sq}(0))-i(\Phi_{00}(L)-\Phi_{00}(0))]\} \quad \text{(A3)}$$

according to Eq. (A2). As we discussed in Sec. III, when the cavity is driven by

$$u_{00}=\begin{pmatrix}1\\0\end{pmatrix}=\begin{pmatrix}1\\ \frac{-ikw(0)\theta'}{1-e^{2i\eta}}\end{pmatrix}+\frac{ikw(0)\theta'}{1-e^{2i\eta}}\begin{pmatrix}\frac{-ikw(0)\theta'}{1-e^{-2i\eta}}\\1\end{pmatrix}$$
$$=v_1+\frac{ikw(0)\theta'}{1-e^{2i\eta}}v_2, \quad \text{(A4)}$$

the reflected field is

$$v_1^*-\frac{ikw(0)\theta'}{1-e^{2i\eta}}v_2^*=\begin{pmatrix}1\\ \frac{ikw(0)\theta'}{1-e^{-2i\eta}}\end{pmatrix}-\frac{ikw(0)\theta'}{1-e^{2i\eta}}\begin{pmatrix}\frac{ikw(0)\theta'}{1-e^{2i\eta}}\\1\end{pmatrix}=\begin{pmatrix}1\\ \frac{kw(0)\theta'}{\tan\eta}\end{pmatrix} \quad \text{(A5)}$$

in a 2×2 model based on $\{u_{00},u_{10}\}$. There are a few observations worth making. First, we can set a limit on the perturbation because

$$kw(0)\theta'\ll\sin\eta,$$

in complete analogy with perturbation theory applied to quantum mechanics. The eigenvectors v_1 and v_2 in Eq. (A4) are not real. This is due to the new wave front that must

match the tilted mirror at $z=0$. In Eq. (A5) the cavity eigenvectors are reflected as conjugate. This comes from the properties of $\hat{L}$, which is symmetric. The reflection from the antireflective surface of the input mirror is represented by $\hat{M}=e^{ik|\vec{r}|^2/R_1}$. If there is no loss,

$$\hat{L}^*(\hat{M}|u_n\rangle)=\hat{M}(\hat{L}^{-1}|u_n\rangle)=\lambda_n^{-1}\hat{M}|u_n\rangle \tag{A6}$$

implying $\hat{M}|u_n\rangle\propto|u_n^*\rangle$. This applies to the perturbed shapes of the input mirror's surface as well. The property $\hat{L}^\dagger\hat{L}=1$ implies that energy is conserved and conjugation upon reflection reveals that there is time-reversal symmetry. In Eq. (A6) $\lambda_n^{-1}=\lambda_n^*$. We also assumed that v_1 was the resonating mode reflected by $+1$ and v_2 nonresonating. The case of both v_1 and v_2 resonating can occur only in a degenerate cavity. Both v_1 and v_2 can be nonresonating. In this case, the reflected beam is

$$\begin{aligned}-v_1^*-\frac{ikw(0)\theta'}{1-e^{2i\eta}}v_2^*=&-\begin{pmatrix}1\\ \dfrac{ikw(0)\theta'}{1-e^{-2i\eta}}\end{pmatrix}\\ &-\frac{ikw(0)\theta'}{1-e^{2i\eta}}\begin{pmatrix}\dfrac{ikw(0)\theta'}{1-e^{2i\eta}}\\ 1\end{pmatrix}\\ =&-\begin{pmatrix}1\\ ikw(0)\theta'\end{pmatrix}\end{aligned} \tag{A7}$$

which represents the vector $-\hat{M}u_{00}$. The minus sign in Eq. (A7) is due to the convention that assigns a positive reflectivity to the reflective side of the mirrors and a negative one to the antireflective side. We can use Eqs. (A5) and (A7) and take the beat between them. The wave number k in Eq. (A7) must be sligthly different from the one in Eq. (A5).

When we place a photodetector in front of the input mirror, we detect a signal proportional to the subtraction of the light impinging on the two half planes $x>0$ and $x<0$. When both the front and the back mirrors are tilted, the signal

$$S\propto\frac{kw(0)\theta'\cos(\eta+\overline{\eta})+kw(L)\theta\cos(\overline{\eta})}{\sin(\eta)} \tag{A8}$$

is proportional to the two angle errors. The phase $\overline{\eta}$ in Eq. (A8) depends on the distance between the input mirror and the photodetector and it corresponds to the phase shift acquired in propagation by the different modes, as in Eq. (A3).

APPENDIX B: THE FAST FOURIER TRANSFORM MODEL USED TO SIMULATE THE SYSTEM

One of the tools that has been used in the LIGO for simulating the interferometer is a FORTRAN implementation of a fast Fourier transform model. The first model was designed by Hello and Vinet to simulate the system when realistic mirrors are included; it was aimed to investigate the impact of distortions on the optical path on the beam, through reflection upon the mirror's surface, and through transmission through their bulk. Since the propagation between the mirrors is calculated by using the paraxial approximation, the field is transformed in the frequency domain to make it propagate, by multiplication with the operator representing the Fourier transform of the propagator. The field is transformed back to the space domain after any propagation, since its interaction with the mirrors is evaluated in the space domain. Each pixel of the grid is multiplied by a phase delay, due to the profile of the mirror along the direction of that pixel. In other words, each pixel of the electromagnetic field couples with the pixel of the mirror map that is right in front of it. This interaction assumes that the light rays do not interfere with each other, when the electromagnetic field interacts with the mirror; the optical path involved in such an interaction is so small that any diffractive coupling between the light rays is neglected.

This code has been widely used in VIRGO and it is part of the numerical tools making up the global simulator of the gravitational wave antenna. Because of its flexibility it has been adapted to simulate the LIGO configuration. A very important feature of this model is that it is a general purpose program, which can be used for studying how power builds up inside each cavity of the system, for any kind of mirror. For example, it has been used for setting requirements and tolerances for the initial LIGO optical components and it showed itself an ideal tool for a quantitative analysis of the effects of thermal lensing. When stationarity is achieved the grids representing the fields are obtained. These data have been manipulated for obtaining information on how the beam becomes distorted because of misalignment or imperfections in the reflecting surfaces.

These grids are represented by 128×128 maps. They contain the imaginary and real parts of the electromagnetic field, picked up at many locations inside and outside the interferometer [20]. The parameters we used in the simulations are the ones currently assumed as standard for the advanced LIGO. We kept fixed the reflectivities of each mirror and the lengths of the cavities according to the advanced LIGO design. When spherical mirrors are implemented,

$$h(x,y)=\sqrt{x^2+y^2}/(2R)$$

stands for the height of the mirror with R the radius of curvature. The grid for any arbitrary shape can be introduced. The ones that have been computed to be implemented in the FFT simulations are designed to match the phase profile of the flat topped beam. The data representing the figure errors of the mirror height are added to the unperturbed profile. For example, when one of the mirrors is tilted by θ around the axis directed along the azimuthal angle ϕ, the perturbation is

$$\delta h(x,y)=\theta[x\sin\phi-y\cos\phi]$$

for a very small misalignment.

[1] F. Bondu, P. Hello, and J. Y. Vinet Phys. Lett. A **246**, 227 (1998).
[2] V. B. Braginsky, M. L. Gorodetsky, and S. P. Vyatchanin Phys. Lett. A **264**, 1 (1999).
[3] Y. T. Liu and K. S. Thorne, Phys. Rev. D **62**, 122002 (2000).
[4] V. Braginsky *et al.*, LIGO Report No. G010333-00-D, 2001; E. D'Ambrosio, LIGO Report No. G010297-00-D, 2001, available at http://www.ligo.caltech.edu at the Document Control Center page.
[5] E. D'Ambrosio, LIGO Report No. T010093-00-D, 2001.
[6] E. D'Ambrosio, R. O'Shaughnessy, S. Strigin, K. Thorne, and S.P. Vyatchanin (in preparation).
[7] We thank Robert Spero for having outlined this issue (private communication).
[8] The current baseline design can be surveyed in P. Fritschel, LIGO Report No. T010075-00-D, 2001, www.ligo.caltech.edu/ligo2
[9] P. A. Belánger and C. Paré, Opt. Lett. **16**, 1057 (1991).
[10] P. A. Belánger, R. L. Lachance, and C. Paré, Opt. Lett. **17**, 739 (1992).
[11] C. Paré and P. A. Belánger, IEEE J. Quantum Electron. **28**, 355 (1992).
[12] H. Kogelnik and T. Li, Appl. Opt. **5**, 1550 (1966).
[13] VIRGO Collaboration, VIRGO Final Design Report No. VIR-TRE-1000-13, 1997.
[14] P. Fritschel *et al.*, Appl. Opt. **37**, 6734 (1998).
[15] Y. Hefetz, N. Mavalvala, and D. Sigg, J. Opt. Soc. Am. B **14**, 1597 (1997).
[16] C.J. Walsh *et al.*, Appl. Opt. **38**, 2870 (1999).
[17] For technical details see E. Black *et al.*, LIGO Report No. T990094-00-D, 1999; E. Black, LIGO Report No. T990093-00-D, 1999.
[18] M. Rakhmanov, Appl. Opt. **40**, 1942 (2001).
[19] R. Beausoleil *et al.*, J. Opt. Soc. Am. B (to be published).
[20] B. Bochner, Ph.D. thesis, MIT, 1998, and references therein.